

MicroRNA Processing Pathway Regulates Olfactory Neuron Morphogenesis

Daniela Berdnik,¹ Audrey P. Fan,¹ Christopher J. Potter,¹ and Liqun Luo^{1,*}

¹Howard Hughes Medical Institute
Department of Biology
Stanford University
Stanford, CA 94305
USA

Summary

The microRNA (miRNA) processing pathway produces miRNAs as posttranscriptional regulators of gene expression. The nuclear RNase III Droscha catalyzes the first processing step together with the dsRNA binding protein DGCR8/Pasha generating pre-miRNAs [1, 2]. The next cleavage employs the cytoplasmic RNase III Dicer producing miRNA duplexes [3, 4]. Finally, Argonautes are recruited with miRNAs into an RNA-induced silencing complex for mRNA recognition (Figure 1A). Here, we identify two members of the miRNA pathway, Pasha and Dicer-1, in a forward genetic screen for mutations that disrupt wiring specificity of *Drosophila* olfactory projection neurons (PNs). The olfactory system is built as discrete map of highly stereotyped neuronal connections [5, 6]. Each PN targets dendrites to a specific glomerulus in the antennal lobe and projects axons stereotypically into higher brain centers [7–9]. In selected PN classes, *pasha* and *Dicer-1* mutants cause specific PN dendrite mistargeting in the antennal lobe and altered axonal terminations in higher brain centers. Furthermore, Pasha and Dicer-1 act cell autonomously in postmitotic neurons to regulate dendrite and axon targeting during development. However, Argonaute-1 and Argonaute-2 are dispensable for PN morphogenesis. Our findings suggest a role for the miRNA processing pathway in establishing wiring specificity in the nervous system.

Results and Discussion

pasha and *Dicer-1* Are Required for PN Dendrite Morphogenesis

To identify genes that are essential for dendrite targeting in *Drosophila* olfactory projection neurons (PNs), we performed a MARCM-based mosaic forward genetic screen by using novel *piggyBac* transposon insertions [10]. We uncovered the insertions LL03660 and LL06357, integrated in *pasha* and *Dicer-1*, respectively (Figure 1B). Both alleles are homozygous lethal, likely to be null, and referred to as *pasha*^{-/-} and *Dicer-1*^{-/-} mutants throughout this study. The *pasha*^{-/-} allele is an insertion in the 5' UTR, resulting in undetectable Pasha protein in homozygous mutant neurons (Figure S1 available online). The *Dicer-1*^{-/-} allele is an insertion in the coding region resulting in a truncated 740 amino acid protein lacking the RNase III, PAZ, and dsRNA binding domains.

The MARCM technique [11] allows us to visualize and manipulate PNs in neuroblast and single-cell clones in an

otherwise heterozygous animal. We use Gal4-GH146 [12] to label PNs from three neuroblast lineages, anterodorsal (ad), lateral (l), and ventral (v) PNs [7]. Wild-type (WT) adPNs, lPNs, and vPNs target stereotyped sets of glomeruli in neuroblast clones (Figure 1C₁₋₃). *pasha*^{-/-} PNs show two dendrite morphogenesis defects for all neuroblast clones. First, the dendritic density in most glomeruli is drastically reduced (compare outlined glomeruli in Figures 1C₁ to 1D₁ and 1C₃ to 1D₃). Second, dendritic branches spill into incorrect glomerular classes (arrows in Figure 1D₁₋₂). We observed very similar PN dendritic defects in *Dicer-1*^{-/-} MARCM clones. Outlined glomeruli represent a reduction in dendrites and arrows point to incorrectly innervated glomeruli (Figure 1E₁₋₃).

We confirmed that the transposon insertions in *pasha* and *Dicer-1* are the cause for the mutant phenotype with two further experiments. First, precise excision of both transposons fully revert PN morphogenesis defects (data not shown). Second, expression of UAS-*pasha*-HA or UAS-*Dicer-1* transgenes fully rescued *pasha* or *Dicer-1* mutant PN phenotypes, respectively, in MARCM experiments (compare outlined glomeruli in Figures 1F and 1G to WT in Figure 1C₁). Because Gal4-GH146 is expressed only in postmitotic neurons [13], these experiments also demonstrate that Pasha and Dicer-1 act in postmitotic neurons to regulate dendrite morphogenesis.

As expected, in all rescue experiments, Pasha-HA localizes to the nucleus (Figure 1F₁₋₂ and insets of Figures 2D and 2E) and Dicer-1 is enriched in the cytoplasm of PNs (Figure 1G₁₋₂ and inset of Figure 2F). Endogenous Pasha protein is found ubiquitously in all cell nuclei in the brain center at 18 hr after puparium formation (APF) (Figures S1A and S1B), when PN dendrites organize the proto-antennal lobe prior to olfactory receptor neuron (ORN) axon entry [14]. Moreover, Pasha is undetectable in *pasha*^{-/-} adPNs and DL1 single neurons (yellow outlines in Figures S1C₁-S1D).

Dendrite Targeting in Specific PN Classes

To study dendrite targeting with a better resolution, we examined single-cell MARCM clones. WT DL1 single-cell clones (hereafter referred to as DL1 single neurons) always target a posterior, dorsolateral glomerulus and fill the glomerulus with dendritic branches (Figure 2A). In *pasha*^{-/-} PNs, 17/25 DL1 single neurons show stereotyped mistargeting defects: dendrites innervate DL1 more sparsely and also mistarget to several additional glomeruli (VA7m, VC2, VA6, DL2d, and DL5), all of which are partially innervated (arrowheads in Figure 2B). 8/25 DL1 single neurons spill their dendrites medially to adjacent glomeruli, mostly D and DL5 (data not shown). Again, *Dicer-1* single mutant neurons exhibit similar PN dendrite mistargeting although to a lower frequency. Similar stereotyped mistargeting pattern as in *pasha* mutants occur in 19/35 DL1 single neurons mutant for *Dicer-1* (arrowheads in Figure 2C), 7/35 single neurons show medially spilled dendrites and 9/35 target normally (data not shown). The variation of DL1 phenotypes could be caused by perdurance of WT protein in single-cell mutant clones, which might affect Dicer-1 more than Pasha. The stereotyped DL1 targeting defect was not found in more than 1400 other *piggyBac* insertions screened (unpublished data), supporting the

*Correspondence: lluo@stanford.edu

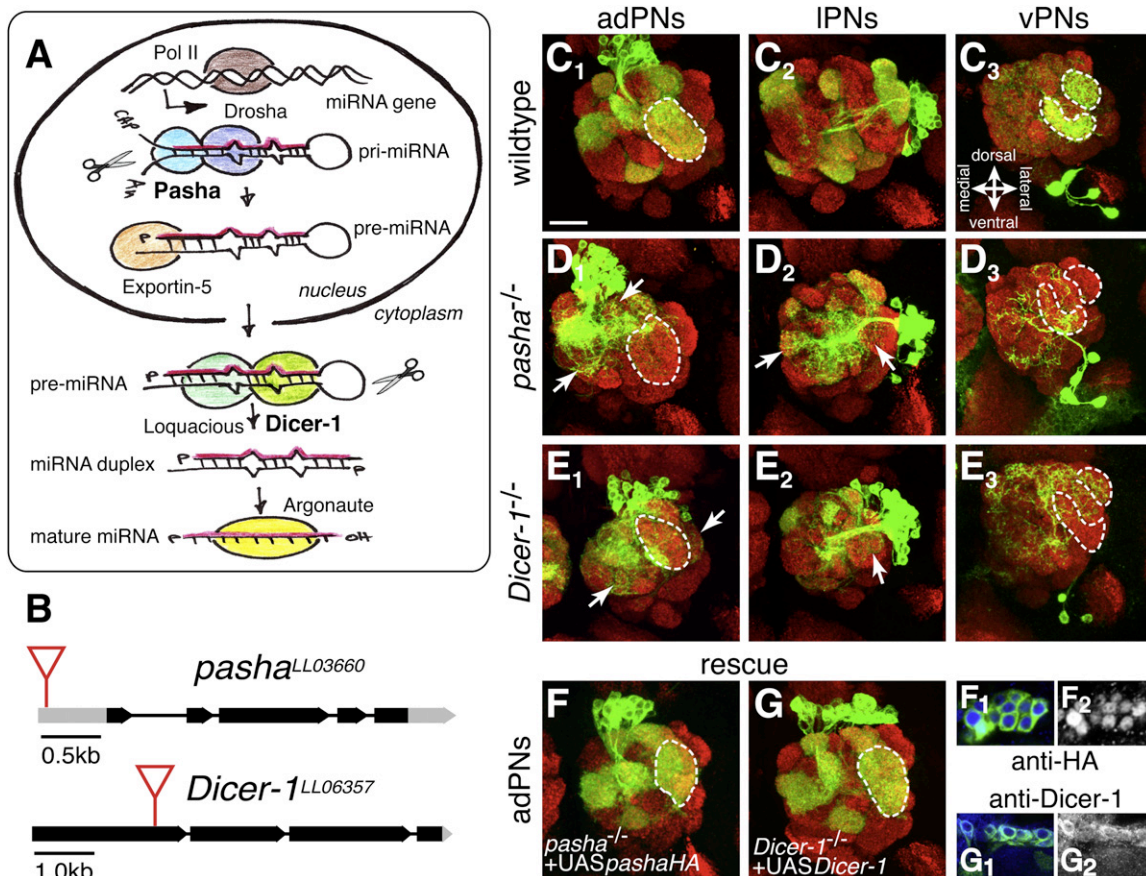


Figure 1. *pasha* and *Dicer-1* Are Required for Dendrite Morphogenesis of Olfactory Projection Neurons

(A) Overview of miRNA-processing pathway. After transcription, pri-miRNA hairpin structures are cleaved by the RNase III enzyme Drosha into a pre-miRNA of about ~70 nt length. Drosha requires the dsRNA binding protein Pasha for this processing step in the nucleus. The pri-miRNA is exported into the cytoplasm by Exportin-5 where it is cleaved into a ~21 nt long miRNA duplex by the RNase III enzyme Dicer-1. The mature single-stranded miRNA is subsequently loaded into the Argonaute-containing RNAi-induced silencing complex (RISC) that binds to complementary mRNAs to regulate translation.

(B) Genomic organization of the *pasha* and *Dicer-1* gene. Black bars represent coding and gray bars noncoding exons and the lines represent introns. Red triangles indicate the insertion sites of the *piggyBac* transposons LL03660 and LL06357. The insertion in *pasha* is in the 5'UTR 515 bp upstream from the start codon. The insertion in *Dicer-1* is in the first exon 2220 bp 3' of the start codon.

(C) WT adPNs (C₁), IPNs (C₂), and vPNs (C₃) target dendrites to stereotypical sets of glomeruli; VA1d and VA1Im adPNs are encircled (C₁), as are DA1 and VA1Im vPNs (C₃).

(D) *pasha*^{-/-} adPNs (D₁), IPNs (D₂), and vPNs (D₃) exhibit severe dendrite targeting defects, with a general reduction in dendritic mass (compare encircled glomeruli in [D₁] and [D₃] to WT in [C₁] and [C₃]) and spilling of dendrites into inappropriate areas (arrows in [D₁₋₂]).

(E) *Dicer-1*^{-/-} PN show very similar targeting defects like *pasha*^{-/-} PNs.

(F and G) PN mutant phenotypes can be rescued completely by expressing either UAS-*pasha*-HA in *pasha*^{-/-} mutant PNs (F) or UAS-*Dicer-1* in *Dicer-1*^{-/-} PNs (G). Pasha-HA localizes to the nucleus (F₂), whereas Dicer-1 is enriched in the cytoplasm (G₂) of PNs.

Green is mCD8-GFP-labeled MARCM clones, red is the presynaptic marker nc82, and blue is anti-HA (F₁) or anti-Dicer-1 (G₁), respectively. Scale bar represents 20 μm. All images are z-projections of confocal stacks except in (F₁), (F₂), (G₁), and (G₂), which are single sections.

specificity of the mutant phenotype for the miRNA processing pathway.

MARCM expression of UAS-Pasha-HA in *pasha*^{-/-} or UAS-Dicer-1 in *Dicer-1*^{-/-} DL1 single neurons fully rescued dendrite targeting (8/8 for *pasha*-HA rescue, Figure 2E; 4/4 for *Dicer-1* rescue, Figure 2F), as is the case of neuroblast clones (Figures 1F and 1G). These experiments demonstrate that Pasha and Dicer-1 act cell autonomously in postmitotic neurons to regulate DL1 dendrite targeting.

To expand the studies of dendrite targeting to other specific PN classes, we used Gal4-Mz19 to label fewer neurons in neuroblast clones [14]. This Gal4 line labels ~6 adPNs that innervate VA1d (asterisk) and DC3 (posterior to VA1d) in WT (Figure 2G). In 21/21 *pasha*^{-/-} adPNs, VA1d/DC3 is sparsely innervated and dendrites are incorrectly targeted to variable

glomeruli such as DA1, VA2, and VM7 (arrowheads in Figure 2H). 23/25 *Dicer-1*^{-/-} PNs show similar medial mistargeting phenotypes albeit to a milder extent, innervating less distant glomeruli (arrowheads in Figure 2I). Similarly, the dendritic density is reduced and incorrect glomeruli are innervated, as in GH146 MARCM experiments (Figures 1D and 1E). Gal4-Mz19 is also expressed in ~7 IPNs innervating the dorsolateral DA1 glomerulus in WT (Figure 2J). DA1 PN targeting is much less affected in *pasha* and *Dicer-1* mutants. 4/5 *pasha* mutant and 7/9 *Dicer-1* mutant IPNs target normally to DA1 with WT dendrite densities (Figures 2K and 2L), whereas 1/5 and 2/9 IPNs exhibit additional partial innervation of the adjacent DL3 glomerulus, respectively (data not shown). Thus, Pasha and Dicer-1 are not required equally in all PN classes, suggesting that potential miRNAs

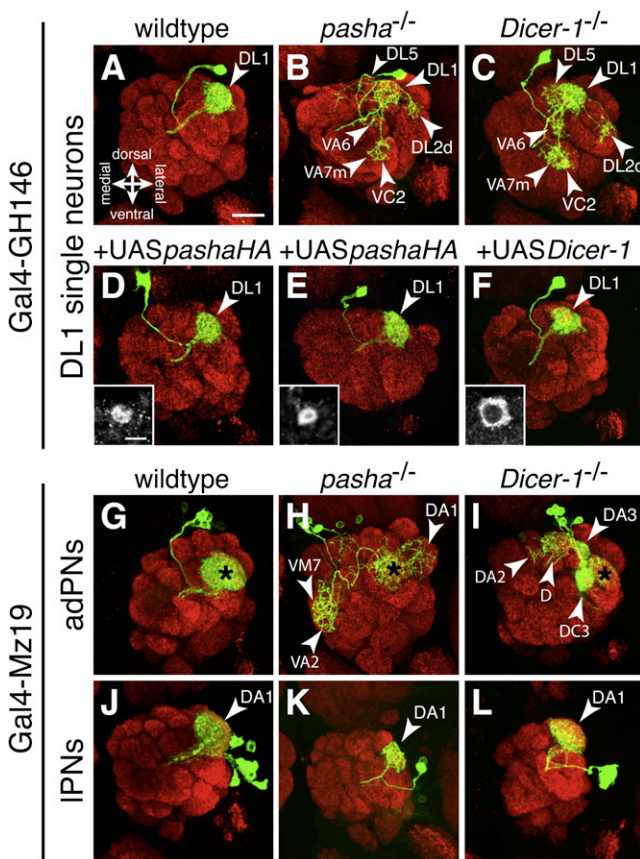


Figure 2. *pasha* and *Dicer-1* Mutants Cause Dendrite Targeting Defects in Specific PNs

(A) WT adPN single-cell clone densely innervates DL1, a dorsolateral posterior glomerulus (arrowhead).

(B) *pasha*^{-/-} DL1 single neurons typically innervate DL1 more sparsely, and also mistarget to five additional glomeruli (VA7m, VC2, VA6, DL5, and DL2d) that are only partially innervated (arrowheads).

(C) Similar DL1 single-neuron phenotypes are seen in *Dicer-1*^{-/-} PNs (arrowheads).

(D) Overexpression of Pasha-HA in WT DL1 single-neurons results in normal dendrite targeting.

(E and F) Expressing either Pasha-HA in *pasha*^{-/-} DL1 single neurons or *Dicer-1* in *Dicer-1*^{-/-} DL1 single neurons rescues the DL1 mistargeting phenotype completely.

(G) In WT MARCM clones, Mz19⁺ adPNs innervate the glomeruli VA1d (asterisk) and DC3 (posterior to VA1d).

(H) In *pasha*^{-/-} Mz19⁺ adPNs, the dendritic mass in VA1d and DC3 is markedly reduced and additional glomeruli are innervated, such as DA1, VM7, and VA2 (arrowheads).

(I) *Dicer-1*^{-/-} Mz19⁺ adPNs sparsely innervate the VA1d glomerulus and mistarget dendrites to incorrect glomeruli, such as DA3, D, and DA2 (arrowheads). The innervation pattern targeting additional glomeruli varies for *pasha*^{-/-} and *Dicer-1*^{-/-} adPNs but is always restricted to the dorsal half of the antennal lobe.

(J) In WT, Mz19⁺ IPN MARCM clones innervate a single dorsolateral glomerulus, DA1 (arrowhead).

(K and L) In *pasha*^{-/-} (K) and *Dicer-1*^{-/-} (L) Mz19⁺ IPNs, the dendritic density in DA1 is equal to WT and no additional glomeruli are innervated in most samples examined.

Green is mCD8-GFP-labeled PNs and their dendrites generated by MARCM using either Gal4-GH146 or -Mz19, red is the presynaptic marker nc82. Insets in (D) and (E) represent anti-HA, and in (F) anti-Dicer-1 stainings in corresponding PNs, respectively. Scale bars represent 20 μm for color images and 5 μm for insets in (D), (E), and (F). Color images are z-projections of confocal stacks, insets are single confocal sections of cell bodies.

might selectively regulate the targeting of specific classes of PNs.

Pasha and Dicer-1 Regulate Axon-Terminal Arborization

In addition to dendrite mistargeting, we also observed axon defects in *pasha* and *Dicer-1* mutants. WT DL1 axons project into the lateral horn (LH) via the mushroom body calyx (MBC) where they form several collateral branches. After entering the LH, DL1 axons always form one characteristic dorsal branch whereas the main branch terminates at the lateral edge of the LH (arrow and arrowhead, respectively, Figure 3A) [8, 9]. In *pasha* and *Dicer-1* mutant DL1 single neurons, axons extend along the normal pathway, form collaterals in the MBC, and always reach the LH. However, more than half of the mutant DL1 axons do not reach the lateral edge but stop within the LH (arrowheads in Figures 3B and 3C). The dorsal branch in the LH is either absent (arrow in Figure 3C) or reduced in length (arrow in Figure 3B). Adding one copy of a UAS-*pasha*-HA transgene in *pasha* (data not shown) or UAS-*Dicer-1* in *Dicer-1* mutant DL1 single neurons rescued all axon phenotypes: the main branch fully extends to the lateral edge of the LH and the dorsal branch is indistinguishable from WT (arrowhead and arrow, respectively, in Figure 3D). Thus, Pasha and Dicer-1 cell autonomously regulate PN axon-terminal elaboration.

pasha Mutant Dendrite Defects Are Manifested during Development

To determine whether the PN dendrite targeting errors are a result of initial mistargeting or failure to maintain stable synaptic connections later, we performed developmental studies. At 18 hr APF, when ORN axons have not yet entered the proto-antennal lobe [14], WT adPN, IPN (Figure 4A₁₋₂), and vPN (not shown) dendrites have already occupied a large area of the proto-antennal lobe (encircled and labeled with N-Cadherin antibodies in red). DL1 single neurons already target their dendrites in the area of the future DL1 glomerulus (arrowhead in Figure 4A₃). In *pasha*^{-/-} PNs, dendritic elaboration within the proto-antennal lobe is extremely reduced in all neuroblast or DL1 single-cell clones at 18 hr APF (outlined in Figure 4B₁₋₃). At 50 hr APF, glomeruli become first visible [14]. In WT adPNs, IPNs, and DL1 single neurons, the same stereotyped innervation patterns as in adults are already evident even though the antennal lobe is smaller in its overall size (compare Figure 1C₁₋₂ to 4C₁₋₂ and Figure 2A to 4C₃). Dendrites of *pasha*^{-/-} PNs are reduced in density (encircled in Figure 4D₁) and spill into lineage-inappropriate glomeruli (arrowheads in Figure 4D₁₋₂). Moreover, stereotyped mistargeting of DL1 single neurons is already evident in 4/4 *pasha*^{-/-} PNs at 50 hr APF (compare arrowheads in Figure 4D₃ with Figure 2B).

These data, in combination with our observation that *pasha* mutant PN dendrite phenotypes do not vary in brains of 3- and 10-day-old adults (data not shown) indicate that Pasha regulates dendrite elaboration and correct targeting early during development.

Dicer-1, but Not Dicer-2, Is Required for PN Targeting

Dicer functions in small RNA maturation across species. *Dicer* mutants are defective for both transcript destruction and translational repression, suggesting that Dicer is required for the siRNA (small interfering RNA) and miRNA maturation pathway [4, 15]. However, the *Drosophila* genome contains two *Dicer* genes, *Dicer-1* and *Dicer-2*, that share similar protein domains but are different in their functions. *Dicer-1* and *Dicer-2*

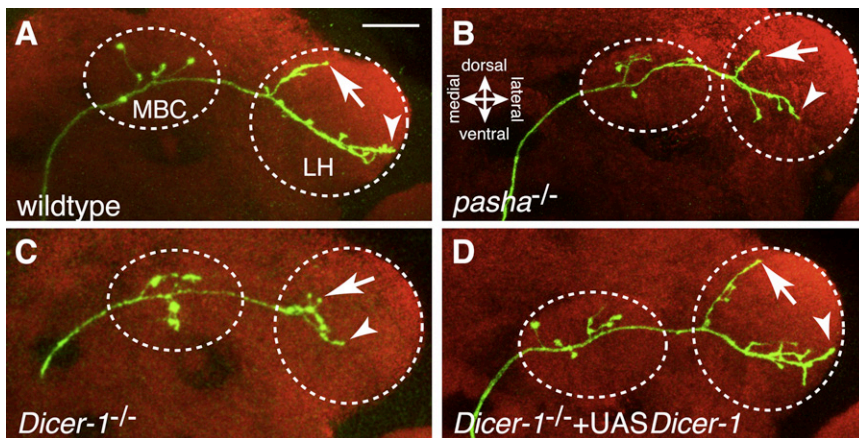


Figure 3. *Pasha* and *Dicer-1* Mutants Affect Axon Termination in the Lateral Horn

(A) WT DL1 PNs project their axons in a stereotypical pattern to the mushroom body calyx (MBC), where they form collateral branches, and to the lateral horn (LH) with a characteristic dorsal (arrow) and main lateral (arrowhead) branch. (B and C) *pasha*^{-/-} and *Dicer-1*^{-/-} DL1 axons project into the LH but the main branches do not reach the lateral edge of the LH (arrowheads). Moreover, the dorsal branch is shorter or absent (arrow). (D) All mutant phenotypes in axons can be fully rescued by expressing *Dicer-1* in *Dicer-1*^{-/-} DL1 single neurons. Green is mCD8-GFP-labeled PN axons, red is the presynaptic marker nc82. Scale bar represents 20 μ m. All images are z-projections of confocal stacks.

are both required for siRNA-dependent mRNA cleavage, with *Dicer-2* acting in siRNA processing and *Dicer-1* acting downstream of siRNA production. However, *Dicer-1*, but not *Dicer-2*, is essential for miRNA-induced silencing during translational repression [16].

To test whether the siRNA processing pathway is required for PN targeting, we made use of *Dicer-2*^{L811fsX} mutants that lack the two RNase III domains essential for dsRNA processing [16]. We found that *Dicer-2*^{L811fsX} mutant PNs exhibit normal dendrite and axon targeting (data not shown), suggesting that *Dicer-2* is dispensable and the siRNA pathway is not required for PN targeting.

Next we asked whether *Dicer-2* could compensate for *Dicer-1*'s function in PN targeting because their protein domain organization is highly similar. We expressed UAS-*Dicer-2* in *Dicer-1*^{-/-} PNs to test whether PN mistargeting phenotypes could be rescued as is the case for UAS-*Dicer-1* expression. We saw no alteration in the *Dicer-1*^{-/-} dendrite mistargeting phenotypes in DL1 PNs (compare arrowheads marking mistargeted glomeruli in Figures S2A₁ and S2B₁), adPNs, or IPNs (compare Figure S2A₂ to S2B₂ and Figure S2A₃ to S2B₃). This observation suggests that *Dicer-2* cannot replace *Dicer-1*'s function during PN targeting. We propose that *Dicer-1*-dependent PN targeting defects are caused by the absence of one or several miRNA(s), because *Dicer-1*, but not *Dicer-2*, is essential for miRNA-directed translation repression and mRNA turnover.

Normal PN Morphogenesis in *AGO1* and *AGO2* Mutants

Many distinct mechanisms have been described for miRNA-mediated gene silencing (reviewed in [17]). However, for all these, the RNA-induced silencing complex (RISC) containing the Argonaute (AGO) proteins as core components is required (Figure 1A). AGO members can be divided into two groups, the ubiquitously expressed AGO and the reproductive cell-specific Piwi subfamily [18, 19]. The AGO subclass containing AGO1 and AGO2 in *Drosophila* is involved in small RNA loading into the RISC. Both miRNAs and siRNAs act as components of RISCs but use different silencing mechanisms. miRNAs typically contain several mismatches when paired with target mRNAs, causing mostly translational repression, whereas siRNAs are perfectly paired with target mRNAs leading to their degradation. AGO2 is described as a multiple-turnover RNA-directed RNA endonuclease acting in mRNA cleavage, whereas AGO1 functions in translational repression but also plays a role in efficient mRNA degradation [20]. However, mRNAs targeted by almost perfectly paired miRNAs can also

be degraded via AGO2 [21, 22]. Thus, AGO1 is typically necessary for stable miRNA maturation and is essential for viability, whereas AGO2 is an essential component of the siRNA-directed RNA interference response [23, 24].

To determine which AGO member is involved in PN targeting, we examined MARCM clones of the strong loss-of-function allele *AGO1*^{k08121} and the *AGO2*⁴¹⁴ null allele [23, 24]. Surprisingly, we observed normal PN dendrite and axon targeting in *AGO1*^{k08121} and *AGO2*⁴¹⁴ adPNs (Figures 5A and 5C compare to WT in Figure 1C₁, and data not shown), and DL1 single neurons as dendrites elaborate in the single dorso-lateral DL1 glomerulus like in WT (arrowheads in Figures 5B and 5D, compare to Figure 2A). To test whether AGO1 and AGO2 could act in a redundant manner, we generated PN clones homozygous mutant for *AGO1* in an *AGO2* homozygous mutant background. 7/7 adPNs and 9/9 DL1 PNs exhibit normal targeting (Figure 5E and arrowhead in Figure 5F). In addition, axon-terminal arborization is normal in *AGO1/AGO2* mutant DL1 cells (data not shown).

There are several explanations for this surprising result. First, the *AGO1*^{k08121} allele may not be null. Second, perdurance of AGO1 protein from parental cells is capable of compensating for the loss of the *AGO1* gene in homozygous mutant clones. *AGO1*^{k08121} mutants have drastically reduced mRNA levels [23], AGO1 is absent in homozygous *AGO1*^{k08121} embryo lysates, and *AGO1*^{k08121} has been shown to disrupt stable miRNA maturation [24]. We also show that in *AGO1*^{k08121} mutant wing disc clones miRNA function is disrupted as in *pasha*^{-/-} and *Dicer-1*^{-/-} clones by using a *bantam* sensor transgene (Figure S3; [25]). Because of these facts and given that WT AGO1 mRNA or protein would be heavily diluted at least in neuroblast clones, the above two explanations imply that a very small amount of AGO1 would be sufficient for PN dendrite targeting. Third, perhaps one or more members of the Piwi subfamily thought to be expressed [20] and function predominantly in the germline could compensate for the loss of AGO1/AGO2 in PNs. However, we observed normal PN morphogenesis in mutants for *piwi*¹ [19] and *aubergine*^{LL06590} [10], and both are Piwi subfamily members (data not shown). Lastly, PN dendrite targeting may utilize a novel miRNA-processing mechanism that is *Dicer-1* dependent but AGO independent.

Conclusion

MicroRNA-mediated posttranslational regulation of gene expression has been documented in an increasing number of biological processes [26]. Many miRNAs are developmentally

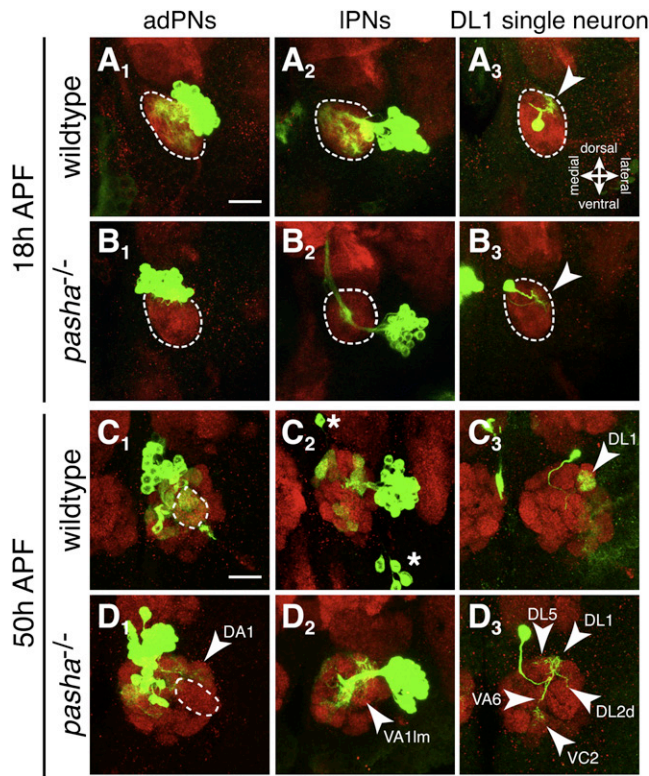


Figure 4. *pasha*^{-/-} Dendrite Targeting Defects Are Manifested during Development

(A) WT adPNs (A₁), IPNs (A₂), and DL1 single neurons (A₃) already exhibit significant dendritic elaboration at 18 hr after puparium formation (APF) in the pupal proto-antennal lobe (encircled).

(B) In *pasha*^{-/-} PNs the dendritic mass is strongly reduced in adPNs (B₁) and IPNs (B₂). Dendrites of DL1 single neurons fail to elaborate on the dorsolateral area where the future DL1 glomerulus will form (compare arrowheads in [A₃] to [B₃]).

(C) At 50 hr APF, WT adPNs (C₁) and IPNs (C₂) already show the stereotypic glomerular innervation of the respective lineages, VA1Im and VA1d being encircled. Dendrites of DL1 single neurons are restricted to a single, dorso-lateral glomerulus (arrowhead in [C₃]).

(D) In *pasha*^{-/-} adPNs and IPNs, the dendritic mass appears strongly reduced (encircled glomeruli in [D₁]) and dendrites target to nonspecific glomeruli (arrowheads in [D₁₋₂]). The DL1 mistargeting phenotype to additional glomeruli like VC2, VA6, DL5, and DL2d is already manifested at 50 hr APF in *pasha* mutants (arrowheads in [D₃]).

Note that in addition to the IPN neuroblast clones, the antennal lobe in (C₂) shows vPNs and a DL1 single neuron (asterisks mark cell bodies). Their dendrites are either masked by overlaying ones in the z-stack (DL1) or weaker in intensity (vPNs).

Green is mCD8-GFP-labeled MARCM clones, red is either anti-N-cadherin labeling the proto-antennal lobe at 18 hr APF (in [A] and [B]) or the presynaptic marker nc82 at 50 hr APF (in [C] and [D]). Scale bars represent 20 μm. All images are z-projections of confocal stacks.

regulated and show tissue-specific expression. In the nervous system, miRNAs have been shown to play roles during neurogenesis, specification of neuronal fate, neuronal morphogenesis, synaptogenesis, and neurodegeneration [27]. We have demonstrated a new function of the miRNA-processing pathway in regulating wiring specificity of the olfactory circuit.

Our results support the model that one or more miRNA(s) are essential for regulating expression of genes that in turn regulate PN dendrite targeting and axon-terminal elaboration in identified neurons during development. Candidate target

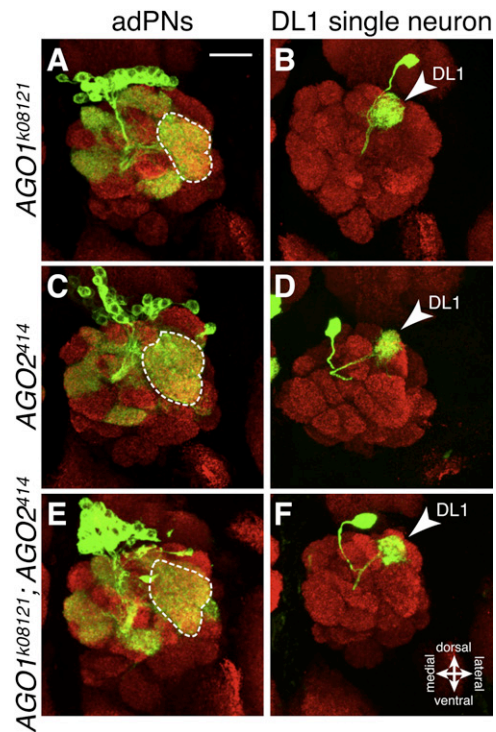


Figure 5. Normal PN Dendrite Targeting in the Absence of AGO-1, AGO-2, or Both

(A and B) *AGO1*^{k08121} adPNs (VA1Im and VA1d are encircled) and DL1 single neurons (arrowhead) exhibit WT PN targeting.

(C and D) *AGO2*⁴¹⁴ adPNs and DL1 single neurons target glomeruli as in WT. (E and F) *AGO1*^{k08121}; *AGO2*⁴¹⁴ double mutant adPNs and DL1 single neurons (arrowhead) cause no defect in glomerular target selection.

Green is mCD8-GFP-labeled MARCM clones, red is the presynaptic marker nc82. Scale bar represents 20 μm. All images are z-projections of confocal stacks.

genes could be transcription factors that regulate wiring specificity in postmitotic neurons, cell-surface receptors for dendrite targeting, or their regulators. Expression or protein levels of such genes are essential for PN dendrite targeting [28, 29]. However, each miRNA is predicted to target hundreds of mRNAs and several miRNAs can regulate one mRNA, adding much more complexity to their regulatory function [30]. Indeed, we tested 7 miRNAs with available null mutants (out of 152 miRNAs predicted in the *Drosophila* genome, see <http://microrna.sanger.ac.uk/sequences>); none of them exhibit PN targeting defects (Table S1). In flies, techniques that would allow the injection of individual or pools of mature miRNAs to rescue the neural phenotypes in *pasha* or *Dicer-1* mutants, or mimic these phenotypes by injecting “target protectors” that interfere with miRNA-mRNA interactions as in zebrafish [31, 32], are currently not available. Therefore, it remains to be a future challenge to identify the miRNA(s), and ultimately their targets, for PN target selection. Looking for mutants with similar phenotypes as *pasha* and *Dicer-1* in forward genetic screens or candidate gene approaches may help to identify specific miRNA and their targets.

Supplemental Data

Supplemental Data include Supplemental Experimental Procedures, three figures, and one table and can be found with this article online at [http://www.current-biology.com/supplemental/S0960-9822\(08\)01275-X](http://www.current-biology.com/supplemental/S0960-9822(08)01275-X).

Acknowledgments

We thank V. Ambros, R. Carthew, S. Cohen, B. Dickson, F.-B. Gao, B. Hay, T. Uemura, and L. Zipursky for fly stocks; G. Hannon and P. Zamore for antibodies; O. Schuldiner and J. Levy for collaboration on the *piggyBac* screen; and F.-B. Gao, K. Wehner, Y.-H. Chou, and O. Schuldiner for comments on the manuscript. This work was supported by fellowships from the Human Frontiers Science Program (D.B.), Damon Runyon Cancer Foundation (C.J.P.), and an NIH grant (R01-DC005982) (L.L.). L.L. is a Howard Hughes Medical Institute Investigator.

Received: April 25, 2008

Revised: September 13, 2008

Accepted: September 17, 2008

Published online: November 13, 2008

References

- Denli, A.M., Tops, B.B., Plasterk, R.H., Ketting, R.F., and Hannon, G.J. (2004). Processing of primary microRNAs by the Microprocessor complex. *Nature* 432, 231–235.
- Gregory, R.I., Yan, K.P., Amuthan, G., Chendrimada, T., Doratotaj, B., Cooch, N., and Shiekhattar, R. (2004). The Microprocessor complex mediates the genesis of microRNAs. *Nature* 432, 235–240.
- Hutvagner, G., McLachlan, J., Pasquinelli, A.E., Balint, E., Tuschl, T., and Zamore, P.D. (2001). A cellular function for the RNA-interference enzyme Dicer in the maturation of the let-7 small temporal RNA. *Science* 293, 834–838.
- Ketting, R.F., Fischer, S.E., Bernstein, E., Sijen, T., Hannon, G.J., and Plasterk, R.H. (2001). Dicer functions in RNA interference and in synthesis of small RNA involved in developmental timing in *C. elegans*. *Genes Dev.* 15, 2654–2659.
- Axel, R. (1995). The molecular logic of smell. *Sci. Am.* 273, 154–159.
- Vosshall, L.B. (2000). Olfaction in *Drosophila*. *Curr. Opin. Neurobiol.* 10, 498–503.
- Jefferis, G.S.X.E., Marin, E.C., Stocker, R.F., and Luo, L. (2001). Target neuron prespecification in the olfactory map of *Drosophila*. *Nature* 414, 204–208.
- Marin, E.C., Jefferis, G.S.X.E., Komiyama, T., Zhu, H., and Luo, L. (2002). Representation of the glomerular olfactory map in the *Drosophila* brain. *Cell* 109, 243–255.
- Wong, A.M., Wang, J.W., and Axel, R. (2002). Spatial representation of the glomerular map in the *Drosophila* protocerebrum. *Cell* 109, 229–241.
- Schuldiner, O., Berdnik, D., Levy, J.M., Wu, J.S., Luginbuhl, D., Gontang, A.C., and Luo, L. (2008). *piggyBac*-based mosaic screen identifies a postmitotic function for cohesin in regulating developmental axon pruning. *Dev. Cell* 14, 227–238.
- Lee, T., and Luo, L. (1999). Mosaic analysis with a repressible cell marker for studies of gene function in neuronal morphogenesis. *Neuron* 22, 451–461.
- Stocker, R.F., Heimbeck, G., Gendre, N., and de Belle, J.S. (1997). Neuroblast ablation in *Drosophila* P[GAL4] lines reveals origins of olfactory interneurons. *J. Neurobiol.* 32, 443–456.
- Spletter, M.L., Liu, J., Su, H., Giniger, E., Komiyama, T., Quake, S., and Luo, L. (2007). *Lola* regulates *Drosophila* olfactory projection neuron identity and targeting specificity. *Neural Develop.* 2, 14.
- Jefferis, G.S., Vyas, R.M., Berdnik, D., Ramaekers, A., Stocker, R.F., Tanaka, N.K., Ito, K., and Luo, L. (2004). Developmental origin of wiring specificity in the olfactory system of *Drosophila*. *Development* 131, 117–130.
- Grishok, A., Pasquinelli, A.E., Conte, D., Li, N., Parrish, S., Ha, I., Baillie, D.L., Fire, A., Ruvkun, G., and Mello, C.C. (2001). Genes and mechanisms related to RNA interference regulate expression of the small temporal RNAs that control *C. elegans* developmental timing. *Cell* 106, 23–34.
- Lee, Y.S., Nakahara, K., Pham, J.W., Kim, K., He, Z., Sontheimer, E.J., and Carthew, R.W. (2004). Distinct roles for *Drosophila* Dicer-1 and Dicer-2 in the siRNA/miRNA silencing pathways. *Cell* 117, 69–81.
- Eulalio, A., Huntzinger, E., and Izaurralde, E. (2008). Getting to the root of miRNA-mediated gene silencing. *Cell* 132, 9–14.
- Hutvagner, G., and Simard, M.J. (2008). Argonaute proteins: Key players in RNA silencing. *Nat. Rev. Mol. Cell Biol.* 9, 22–32.
- Cox, D.N., Chao, A., Baker, J., Chang, L., Qiao, D., and Lin, H. (1998). A novel class of evolutionarily conserved genes defined by piwi are essential for stem cell self-renewal. *Genes Dev.* 12, 3715–3727.
- Williams, R.W., and Rubin, G.M. (2002). ARGONAUTE1 is required for efficient RNA interference in *Drosophila* embryos. *Proc. Natl. Acad. Sci. USA* 99, 6889–6894.
- Miyoshi, K., Tsukumo, H., Nagami, T., Siomi, H., and Siomi, M.C. (2005). Slicer function of *Drosophila* Argonautes and its involvement in RISC formation. *Genes Dev.* 19, 2837–2848.
- Forstemann, K., Horwich, M.D., Wee, L., Tomari, Y., and Zamore, P.D. (2007). *Drosophila* microRNAs are sorted into functionally distinct argonaute complexes after production by dicer-1. *Cell* 130, 287–297.
- Kataoka, Y., Takeichi, M., and Uemura, T. (2001). Developmental roles and molecular characterization of a *Drosophila* homologue of *Arabidopsis* Argonaute1, the founder of a novel gene superfamily. *Genes Cells* 6, 313–325.
- Okamura, K., Ishizuka, A., Siomi, H., and Siomi, M.C. (2004). Distinct roles for Argonaute proteins in small RNA-directed RNA cleavage pathways. *Genes Dev.* 18, 1655–1666.
- Brennecke, J., Hipfner, D.R., Stark, A., Russell, R.B., and Cohen, S.M. (2003). *bantam* encodes a developmentally regulated microRNA that controls cell proliferation and regulates the proapoptotic gene *hid* in *Drosophila*. *Cell* 113, 25–36.
- Bushati, N., and Cohen, S.M. (2007). microRNA functions. *Annu. Rev. Cell Dev. Biol.* 23, 175–205.
- Gao, F.B. (2008). Posttranscriptional control of neuronal development by microRNA networks. *Trends Neurosci.* 31, 20–26.
- Komiyama, T., and Luo, L. (2007). Intrinsic control of precise dendritic targeting by an ensemble of transcription factors. *Curr. Biol.* 17, 278–285.
- Komiyama, T., Sweeney, L.B., Schuldiner, O., Garcia, K.C., and Luo, L. (2007). Graded expression of semaphorin-1a cell-autonomously directs dendritic targeting of olfactory projection neurons. *Cell* 128, 399–410.
- Chen, K., and Rajewsky, N. (2007). The evolution of gene regulation by transcription factors and microRNAs. *Nat. Rev. Genet.* 8, 93–103.
- Schier, A.F., and Giraldez, A.J. (2006). MicroRNA function and mechanism: Insights from zebra fish. *Cold Spring Harb. Symp. Quant. Biol.* 71, 195–203.
- Choi, W.Y., Giraldez, A.J., and Schier, A.F. (2007). Target protectors reveal dampening and balancing of Nodal agonist and antagonist by miR-430. *Science* 318, 271–274.

Supplemental Data

MicroRNA Processing Pathway Regulates

Olfactory Neuron Morphogenesis

Daniela Berdnik, Audrey P. Fan, Christopher J. Potter, and Liqun Luo

Supplemental Experimental Procedures

Fly Stocks and Phenotypic Analysis

The insertions *LL03660* (in *pasha*), *LL06357* (in *Dicer-1*) and *LL06590* (in *aubergine*) originate from a *piggyBac* screen [1]. Information for all other mutant alleles used can be found in Flybase (<http://flybase.bio.indiana.edu>). Mosaic analyses with MARCM were performed as previously described using Gal4-GH146 and -Mz19 [2]. UAS-*Dicer-1* and UAS-*Dicer-2* transgene insertions on the 3rd chromosome and 2nd chromosome, respectively, were used for rescue and other experiments [3].

Transgene Construction

To generate UAS-*pasha-HA*, a full length cDNA (LD23072) was amplified using the following primers (5'-3'): CACCATGGCGGAGAAGCCGCTGGCC and AAGTTCCACGTTGTTCAAATTGGACCC. The PCR product was subcloned into pENTR-D/TOPO (Invitrogen) and recombined into pTWH (Gateway Collection, Drosophila Genomics Resource Center, Bloomington, IN) by using the Gateway LR clonase II enzyme mix (Invitrogen). A UAS-*pasha-HA* transgene insertion on the 2nd chromosome was used for all rescue experiments.

Generation of GH146-Gal4 Transgene

The p[GAL4, w+]^{GH146} enhancer trap was reproduced as a construct by inserting the 5P transposase promoter, GAL4 gene, and hsp70 terminator from pGaWB [4] into a cloned 12.6kb genomic fragment which flanks the p[GAL4, w+]^{GH146} insertion site. The GAL4 gene was inserted into the genomic fragment in the same position and orientation as the p[GAL4, w+]^{GH146} enhancer trap. The entire construct was cloned into a DsRed-marked *piggyBac* transformation vector [1]. A GH146-Gal4 transgene insertion on the X chromosome was used for MARCM experiments on chromosome 2R.

Clonal Analysis Using *bantam* Sensor

Mutant clones of *pasha*, *Dicer-1* and *AGO1* were generated in 3rd instar larval wing discs and assayed for *bantam* miRNA activity using the *bantam* sensor transgene on chromosome 2R (we determined to be at 60A11 by inverse PCR) as described in Brennecke et al. [5]. Discs were stained with anti- β -Galactosidase antibody to mark the clones, anti-GFP to visualize sensor expression and DAPI to mark nuclei. Clones were analyzed by confocal

microscopy and bantam activity was defined as ratios of mean fluorescence intensities of homozygous mutant divided by heterozygous tissue. Confocal images for clonal GFP level quantification in Figure S3 were taken under non-saturating conditions and black values were above 0.

Immunohistochemistry

Fly brains were dissected, fixed, stained and primary antibodies were diluted as described [1, 2, 6]. Rabbit anti-Pasha was used 1:500 [7], rabbit anti-Dicer-1 1:100 [8], chicken anti-GFP 1:500 (Aves Labs, cat.# GFP-1020) and rabbit anti- β -Galactosidase 1:1000 (Cappel, cat.# 55976).

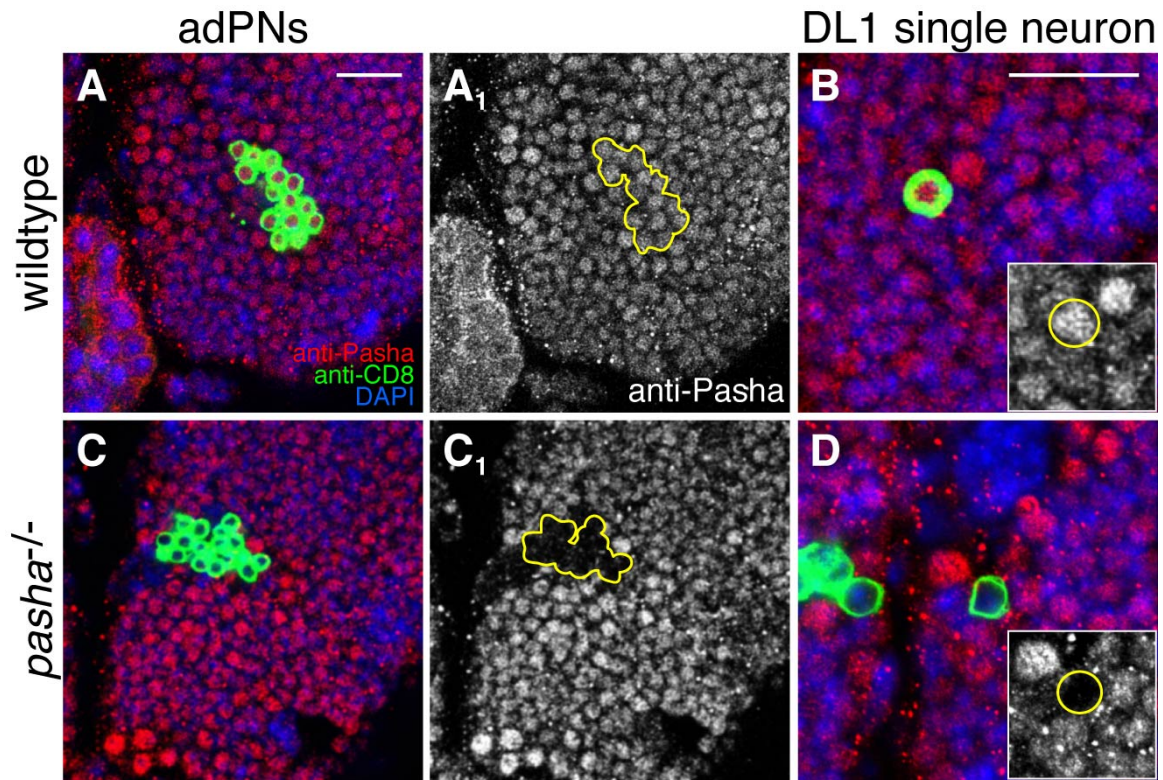


Figure S1. Pasha protein is absent in *pasha*^{-/-} PNs at 18h APF.

(A and B) Pasha localizes to the nucleus of WT adPNs and DL1 single neurons and all surrounding cells in 18h APF pupal brains at equal levels. Pasha staining is shown separately in A₁ for the adPN clone and the inset in B for a single neuron, both outlined in yellow.

(C and D) Pasha protein is absent from *pasha*^{-/-} adPNs (C and C₁) and DL1 single neurons (D and inset) at 18h APF while heterozygous neighboring cells express Pasha in the nucleus. The MARCM clones are outlined in yellow based on GFP-staining; the actual clone may also contain some Gal4-GH146 negative, and hence GFP-negative cells (e.g., in C₁).

Green is mCD8-GFP labeled MARCM clones, red labels anti-Pasha and blue is DAPI. Scale bars represent 20µm. All images are single confocal sections.

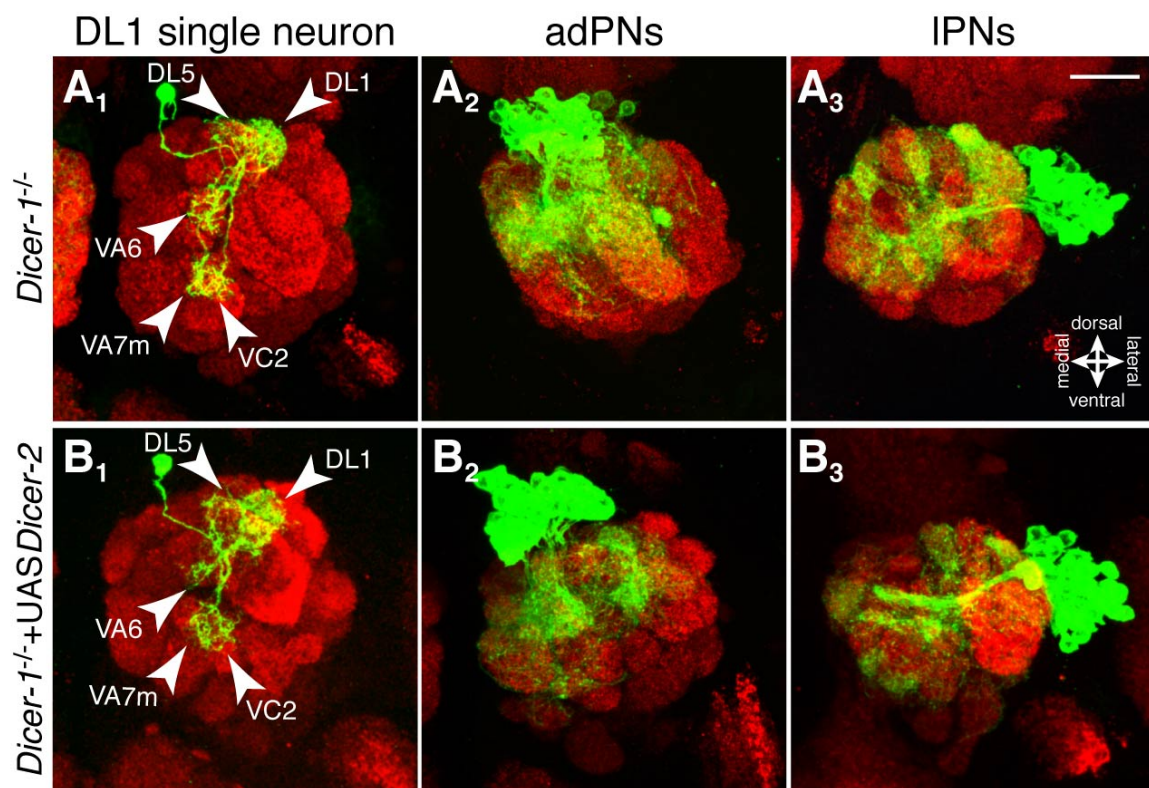


Figure S2. Dicer-2 cannot compensate for Dicer-1 function during PN targeting.

(A₁) In *Dicer-1*^{-/-} DL1 single neurons dendrites mistarget to other glomeruli besides DL1 (arrowheads). In *Dicer-1*^{-/-} adPNs (A₂) and IPNs (A₃) the dendritic mass is significantly reduced and dendrites spill non-specifically into inappropriate glomeruli. All these dendritic phenotypes cannot be rescued or altered by overexpressing Dicer-2 in *Dicer-1*^{-/-} DL1 single neurons (arrowheads in B₁, compare to A₁), adPNs (B₂, compare to A₂), and IPNs (B₃, compare to A₃). Green is mCD8-GFP labeled MARCM clones, red labels the presynaptic marker nc82. Scale bar represents 20μm. All images are z-projections of confocal stacks.

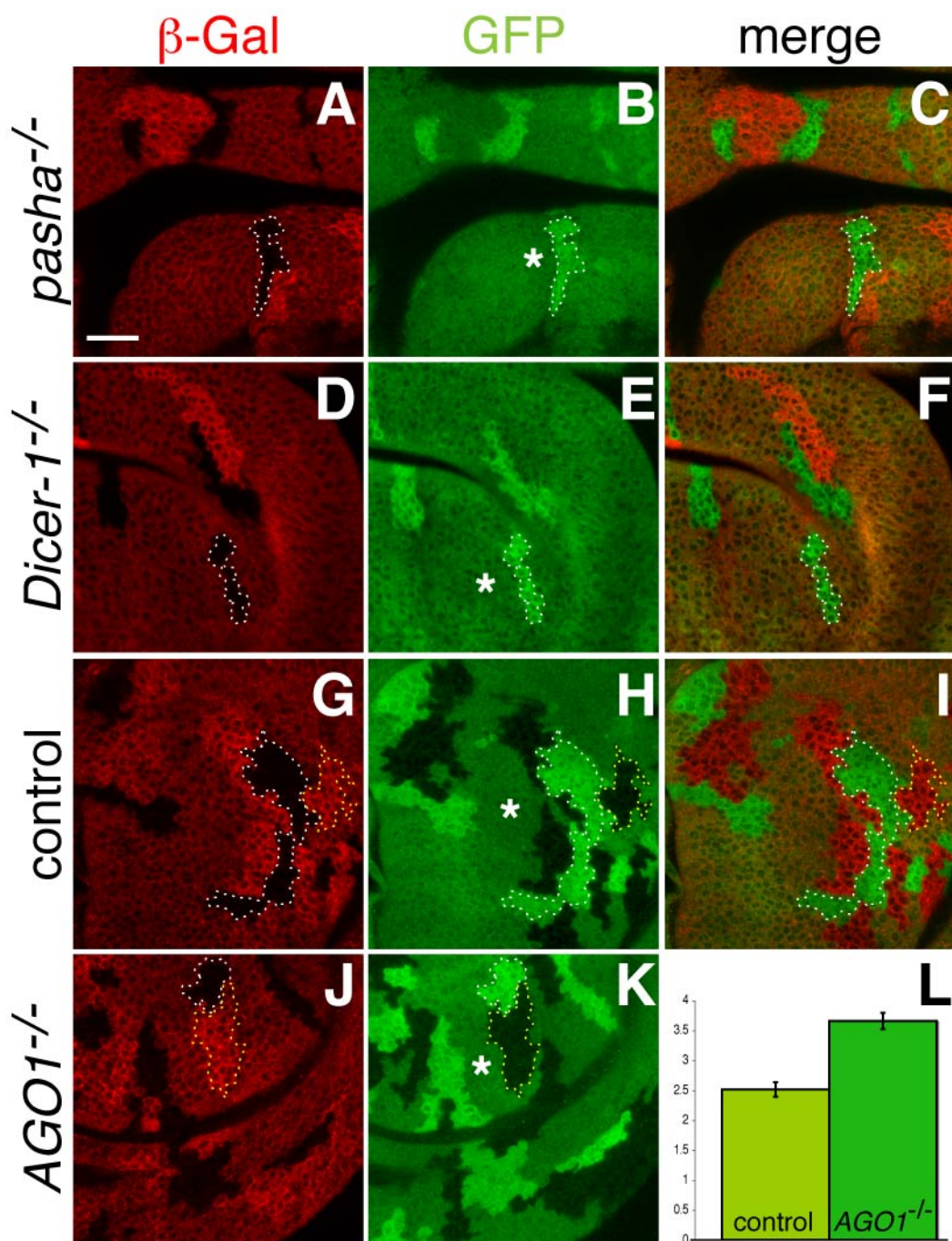


Figure S3. *bantam* sensor is de-repressed in *AGO1*^{k08121} mutant clones of larval wing discs.

(A-C) *pasha*^{-/-} clones are marked by the absence of a *LacZ* reporter gene (red, A). An example is outlined by dashed line. GFP levels are elevated compared to

heterozygous tissue (asterisk), presumably due to the absence of mature miRNA within the clone (B). n=11.

(D-F) In *Dicer-1*^{-/-} clones the effect of *bantam* sensor de-repression is similar. n=12.

(G-K) FRT42D control (G) or FRT42D *AGO1*^{k08121} mutant clones (J), respectively, are marked by the lack of β -Gal staining (examples outlined by white dashed line) and contain two copies of the same *bantam* sensor transgene as in B and E, which is located also on chromosome 2R (H, K). Twin spot clones contain two copies of *LacZ* (examples marked by yellow dashed line) but lack any *bantam* sensor transgene (H, K). Heterozygous tissue bears one copy of *LacZ* and *bantam* sensor transgene and is marked by an asterisk (H, K).

(L) The extent of *bantam* sensor de-repression in *AGO1*^{k08121} mutant clones was determined as follows: we subtracted the mean fluorescence intensity of twin spot clones (no *bantam* sensor) from the homozygous (two copies of *bantam* sensor) and heterozygous clones (one copy of *bantam* sensor) separately, and then calculated the ratio of the homozygous and the heterozygous values. In control clones, *bantam* sensor expression is increased by ~2.5 fold compared to heterozygous tissue. In *AGO1*^{k08121} mutant clones *bantam* sensor expression is up-regulated ~3.7 fold, showing a significant increase in GFP levels compared to the control ($p=1.7 \times 10^{-6}$; n= 13 or 16 independent clones for control or *AGO1*^{k08121} mutants, respectively). Error bars indicate SEM.

Larval genotypes: (A-C) Hs-FLP1; *bantam* sensor/ +; *arm-LacZ* FRT82B/ FRT2A FRT82B *pasha*^{LL03660} y+; (D-F) Hs-FLP1; *bantam* sensor/ +; *arm-LacZ* FRT82B/ FRT2A FRT82B *Dicer-1*^{LL06357} y+; (G-I) Hs-FLP1; FRT42D *bantam* sensor/ FRT42D *arm-LacZ*; (J-K) Hs-FLP1; FRT42D *AGO1*^{k08121} *bantam* sensor/ FRT42D *arm-LacZ*

Green represents *bantam* sensor GFP expression, red anti- β -Galactosidase. Scale bar represents 20 μ m. All images are single confocal sections of 3rd instar wing imaginal discs.

Table S1. Seven miRNA mutants exhibit WT DL1 targeting.

miRNA	allele generated by	reference	WT DL1 targeting*
<i>miR1</i>	homologous recombination	[9]	7/7
<i>miR7</i>	imprecise excision	[10]	10/10
<i>miR8</i>	imprecise excision	[11]	19/19
<i>miR9a</i>	homologous recombination	[12]	14/14
<i>miR14</i>	imprecise excision	[13]	6/6
<i>miR279</i>	P-element insertion	[14]	13/13
<i>bantam</i>	imprecise excision	[5]	6/6

* numbers represent antennal lobes scored for DL1 targeting phenotypes

Supplemental References

1. Schuldiner, O., Berdnik, D., Levy, J.M., Wu, J.S., Luginbuhl, D., Gontang, A.C., and Luo, L. (2008). piggyBac-based mosaic screen identifies a postmitotic function for cohesin in regulating developmental axon pruning. *Dev Cell* *14*, 227-238.
2. Wu, J.S., and Luo, L. (2006). A protocol for mosaic analysis with a repressible cell marker (MARCM) in *Drosophila*. *Nat Protoc* *1*, 2583-2589.
3. Dietzl, G., Chen, D., Schnorrer, F., Su, K.C., Barinova, Y., Fellner, M., Gasser, B., Kinsey, K., Oettel, S., Scheiblaue, S., et al. (2007). A genome-wide transgenic RNAi library for conditional gene inactivation in *Drosophila*. *Nature* *448*, 151-156.
4. Brand, A.H., and Perrimon, N. (1993). Targeted gene expression as a means of altering cell fates and generating dominant phenotypes. *Development* *118*, 401-415.
5. Brennecke, J., Hipfner, D.R., Stark, A., Russell, R.B., and Cohen, S.M. (2003). bantam encodes a developmentally regulated microRNA that controls cell proliferation and regulates the proapoptotic gene hid in *Drosophila*. *Cell* *113*, 25-36.
6. Lee, T., and Luo, L. (1999). Mosaic analysis with a repressible cell marker for studies of gene function in neuronal morphogenesis. *Neuron* *22*, 451-461.
7. Denli, A.M., Tops, B.B., Plasterk, R.H., Ketting, R.F., and Hannon, G.J. (2004). Processing of primary microRNAs by the Microprocessor complex. *Nature* *432*, 231-235.
8. Forstemann, K., Horwich, M.D., Wee, L., Tomari, Y., and Zamore, P.D. (2007). *Drosophila* microRNAs are sorted into functionally distinct argonaute complexes after production by dicer-1. *Cell* *130*, 287-297.
9. Sokol, N.S., and Ambros, V. (2005). Mesodermally expressed *Drosophila* microRNA-1 is regulated by Twist and is required in muscles during larval growth. *Genes Dev* *19*, 2343-2354.
10. Li, X., and Carthew, R.W. (2005). A microRNA mediates EGF receptor signaling and promotes photoreceptor differentiation in the *Drosophila* eye. *Cell* *123*, 1267-1277.
11. Karres, J.S., Hilgers, V., Carrera, I., Treisman, J., and Cohen, S.M. (2007). The conserved microRNA miR-8 tunes atrophin levels to prevent neurodegeneration in *Drosophila*. *Cell* *131*, 136-145.
12. Li, Y., Wang, F., Lee, J.A., and Gao, F.B. (2006). MicroRNA-9a ensures the precise specification of sensory organ precursors in *Drosophila*. *Genes Dev* *20*, 2793-2805.
13. Xu, P., Vernooy, S.Y., Guo, M., and Hay, B.A. (2003). The *Drosophila* microRNA Mir-14 suppresses cell death and is required for normal fat metabolism. *Curr Biol* *13*, 790-795.
14. Cayirlioglu, P., Kadow, I.G., Zhan, X., Okamura, K., Suh, G.S., Gunning, D., Lai, E.C., and Zipursky, S.L. (2008). Hybrid neurons in a microRNA mutant are putative evolutionary intermediates in insect CO₂ sensory systems. *Science* *319*, 1256-1260.